Evaluation of chemical labeling strategies for monitoring HCV RNA using vibrational microscopy†

Matthew Noestheden,[a,b] Qingyan Hu,[a] Angela M. Tonary,[a] Li-Lin Tay[c] and John Paul Pezacki*[a,b]

Received 30th March 2007, Accepted 4th June 2007
First published as an Advance Article on the web 21st June 2007
DOI: 10.1039/b704812b

Raman and coherent anti-Stokes Raman scattering (CARS) microscopies have the potential to aid in detailed longitudinal studies of RNA localization. Here, we evaluate the use of carbon–deuterium and benzonitrile functional group labels as contrast agents for vibrational imaging of hepatitis C virus (HCV) replicon RNA. Dynamic light scattering and atomic force microscopy were used to evaluate the structural consequences of altering HCV subgenomic replicon RNA. Modification with benzonitrile labels caused the replicon RNA tertiary structure to partially unfold. Conversely, deuterium-modified replicon RNA was structurally similar to unmodified replicon RNA. Furthermore, the deuterated replicon RNA provided promising vibrational contrast in Raman imaging experiments. The functional effect of modifying subgenomic HCV replicon RNA was evaluated using the luciferase gene as a genetic reporter of translation. Benzonitrile labeling of the replicon RNA prevented translation in cell-based luciferase assays, while the deuterated replicon RNA retained both translation and replication competency. Thus, while the scattering cross-section for benzonitrile labels was higher, only carbon–deuterium labels proved to be non-perturbative to the function of HCV replicon RNA.

Introduction

First identified in 1989, hepatitis C virus (HCV) is a human pathogen that has developed into a global health problem.[1–3] Much of the recent effort towards understanding HCV pathogenesis has focused on elucidating structural and functional components of the HCV genome and the proteins for which it codes, as well as identifying host–virus interactions that serve as molecular keystones in the HCV life-cycle. However, there is little information pertaining to the *in situ* dynamics of HCV viral processes. This is largely due to a lack of techniques suited to such analyses.

One method of studying HCV *in situ* is to infect primary hepatocytes in cell culture or certain cell lines with HCV-infected sera. Alternatively, culturing primary cells isolated from persistently infected patients can also be performed.[4] While attempts to develop chimpanzee and small animal models of HCV infection met with modest success, recent work has led to the development of a number of cell-based models of HCV replication and infectivity that have become the primary systems used to study the virus.[4–10] Importantly, the *in vitro* transcription (IVT) of HCV subgenomic replicon RNA (HCV RNA; Fig. 1) to accommodate transient expression of viral RNA and proteins, which was the method used in the current study, is known to elicit effects similar to those observed in other infectious models.[11,12]

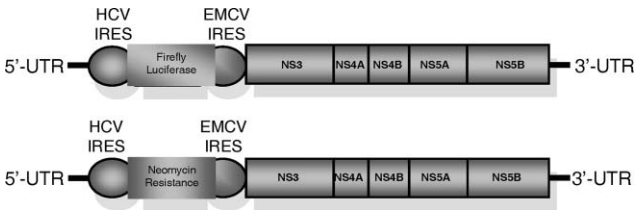

Fig. 1 Schematic representation of the organization of HCV subgenomic replicons. The 5′- and 3′-UTRs and the NS3–NS5B regions are requisite for viral replication in cell culture. Expression of the HCV coding region is driven by the EMCV promoter. Two variants contain either the firefly luciferase reporter gene (top) or the neomycin resistance selection gene (bottom), both of which are controlled by the HCV IRES. UTR = untranslated region; IRES = internal ribosomal entry site; NS3–NS5B region represents the region coding for the HCV polyprotein.

The most common approach to visualizing HCV components in cell culture is to use indirect immunofluorescence.[11–14] However, usually this approach necessitates fixing cells to a substrate prior to staining and imaging, thus providing only static images.[15] To try and obtain real-time information on RNA dynamics in live cells, researchers have developed a variety of techniques based on fluorescence that, due to photobleaching effects, only give information about RNA localization over short timeframes.[16–23] Also noteworthy is the limited number of attempts to directly localize HCV RNA *in vivo*.[12,24] Several groups have used 5-bromouridine-5′-triphosphate metabolic labeling to indirectly localize positive-sense RNA by showing that negative-sense RNA co-localizes with components of the viral replication complex.[19,25] However, new methods applicable to live-cell imaging are required to move beyond static/indirect images of HCV viral processes.

[a]*Steacie Institute for Molecular Sciences, The National Research Council of Canada, 100 Sussex Dr., Ottawa, Ontario, Canada K1A 0R6. E-mail: John.Pezacki@nrc.ca; Fax: +1 (613) 952-0068*
[b]*Department of Chemistry, University of Ottawa, 10 Marie-Curie, Ottawa, Ontario, Canada K1N 6N5*
[c]*Institute for Microstructural Sciences, National Research Council of Canada, 207-1200 Montreal Rd., Ottawa, Ontario, Canada K1A 0R6*

† Electronic supplementary information (ESI) available: Synthesis of benzonitrile labels, HPLC and LC/MS validation procedures, benzonitrile modification of aminoallylated HCV replicon RNA and figures relevant to the above data. See DOI: 10.1039/b704812b

Vibronic imaging modalities such as infrared and Raman imaging offer several advantages over fluorescence-based techniques, the main benefits being that these methods are non-invasive and provide chemically selective image contrast. Disadvantages include slow image acquisition time, and low spatial resolution. Coherent anti-Stokes Raman scattering (CARS) microscopy surmounts these issues and has been used for 3D imaging, at diffraction-limited subcellular resolution, in live cells using the natural spectroscopic (vibrational Raman) signatures of cellular components to generate image contrast.[26] CARS microscopy has also been utilized to investigate changes in the lipid droplet profile of Huh-7 cells containing replicating HCV following treatment with a small molecule that perturbs the HCV life-cycle.[13] In addition, a novel study that combines CARS with two-photon fluorescence to simultaneously examine the localization of HCV RNA and the changes in lipid homeostasis associated with viral replication and translation has been conducted.[24]

In order to track specific biomolecules in real-time *in vivo* using Raman/CARS microscopy, there must be a mechanism of generating image contrast that is unique to particular biomolecules. Achieving this requirement necessitates the incorporation of exogenous Raman labels to specific biomolecules. Such Raman labels should possess the following desirable properties: 1) they should present a Raman signature that is orthogonal to all endogenous Raman modes; 2) covalent attachment of the probe should be easy and reproducible; 3) they should be chemically inert in a biological context; and 4) the structure of the Raman mode should enable the lowest possible detection limit with current instrumentation (*i.e.*, it should have a high Raman scattering cross-section). Nitrile (CN) groups have been used previously for modifying proteins for various applications and have favorable properties, as do carbon–deuterium (C–D) bonds.[26–29] Herein, we describe the incorporation of both CN and C–D vibrational resonances as Raman labels for the functionalization of HCV replicon RNA. The HCV RNA construct used for this study is large and contains many functionally integral secondary and tertiary structural elements that could be perturbed upon functionalizing the RNA. Therefore, we performed detailed studies of the deuterated and nitrile-functionalized HCV RNA to evaluate which strategy may be most suitable for generating image contrast while retaining viral RNA function.

Results and discussion

An obvious choice to generate vibrational contrast would be to exploit the O–P–O nucleotide backbone mode (~1090 cm^{-1}), which is spectrally well-resolved and has a strong scattering cross-section. However, the presence of endogenous O–P–O modes precludes resolving host-cell from replicon RNA resonances. To determine where unique vibrational contrast could be introduced, the Raman spectrum of homogenized Huh-7 hepatoma cells was examined (Fig. 2). An important feature of this spectrum is the Raman-transparent region from 1800 to 2700 cm^{-1}. Raman resonances in this region are generally cumulene (CO_2, ketene, *etc.*) or triple-bonded (acetylenes, molecular nitrogen, azides and nitrile) systems. Also of note is the C–D vibrational resonance around 2200 cm^{-1}. Our study focuses on the CN and C–D groups as contrast agents because of their biostability and the ease of functionalizing HCV replicon RNA with these vibrational modes.

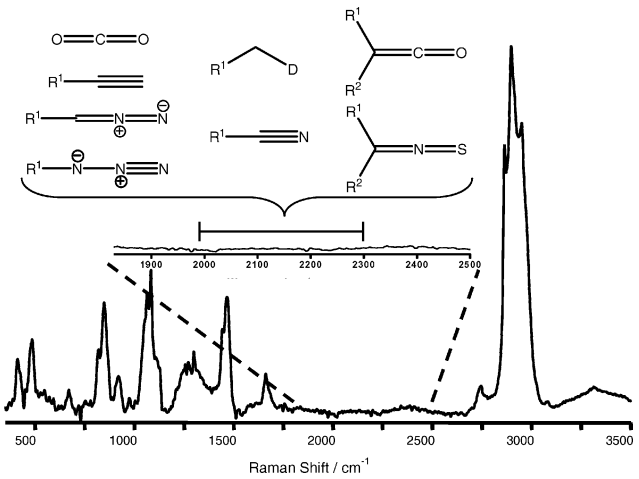

Fig. 2 Designing Raman and CARS contrast agents. The Raman-transparent region from 1800 to 2700 cm^{-1} contains a variety of Raman modes that could be used to develop CARS contrast agents. When weighed against all other considerations, the C–D and CN modes are the most amenable to this task. The spectrum was integrated over 30 sec. R^1, R^2 = contrast agent scaffold.

Preparation and characterization of fully deuterated HCV RNA (D-HCV RNA)

Deuterium does not have additional steric requirements over that of hydrogen. As such, incorporating deuterium into structurally complex molecules (*i.e.*, HCV RNA) was attempted to determine if such substitutions elicit any functional and structural perturbations. The substitution of deuterium for hydrogen does not implicitly require the addition of exogenous functional groups to facilitate conjugation of a deuterated probe to the biomolecule. Rather, deuterated building blocks can be fed to an organism or used *in vitro* to enzymatically synthesize deuterium-modified biomacromolecules.[30–32] The synthesis of D-HCV RNA was successfully accomplished using deuterated nucleotides as components in the IVT reaction (Fig. 3). The yields of D-HCV RNA were 80–90% relative to those of normal HCV RNA

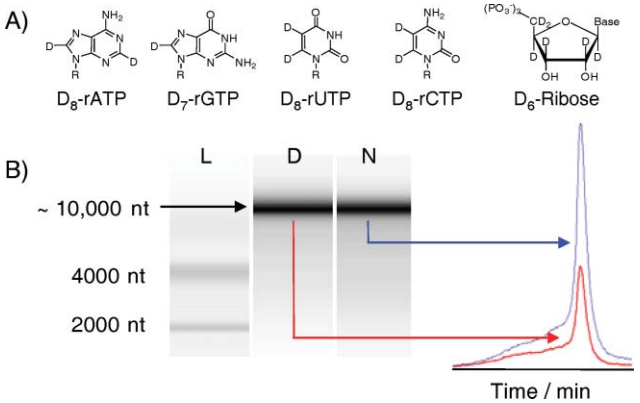

Fig. 3 Validation of D-HCV RNA synthesis. A) Deuterium substitutions in the nucleobase and ribose sugars that will be used as CARS contrast agents. R = nucleotide backbone. B) Electrophoretic migration (left) of HCV RNA (N) and D-HCV RNA (D) were identical, indicating that the D-HCV RNA reaction produced a full-length (~10 000 nt) transcript population. The electropherograms (right) illustrate the lack of early termination products for HCV RNA and D-HCV RNA. L = RNA ladder.

transcripts, which is reasonable when compared to the yields of other IVT reactions using modified substrates (45–100%).[33–36]

Raman spectroscopic analysis showed that D-HCV RNA retained all the spectroscopic information of HCV RNA from 1050–2000 cm^{-1}. However, the entire aliphatic region shifted into the Raman transparent window of the cell, which was conclusive evidence that deuterated nucleotides were incorporated during the IVT reaction (Fig. 4). In addition to the C–D modes from 2050–2300 cm^{-1}, the presence of the O–P–O nucleotide backbone resonance (1090 cm^{-1}) gave confirmation that it was the D-HCV RNA being analyzed and not residual D-rNTPs. The spectroscopic data also illustrated that the bulk scattering cross-section of the C–D mode can be quite prominent despite the weak cross-section of individual C–D modes. Raman imaging of D-HCV RNA showed that contrast specific to the C–D mode was generated. Subsequent attempts to localize D-HCV RNA *in vivo* were hindered due to the limited sensitivity of Raman microscopy under cellular imaging conditions. Future work will focus on tracking D-HCV RNA with CARS microscopy, which is several orders of magnitude more sensitive than Raman. Quantitative analysis of the C–D cross-section was not performed due to the logistics of obtaining samples with consistent thickness. Regardless, this proof-of-principle *in vitro* experiment showed that D-HCV RNA has the potential to function as a tool in the study of HCV RNA using Raman/CARS microscopy.

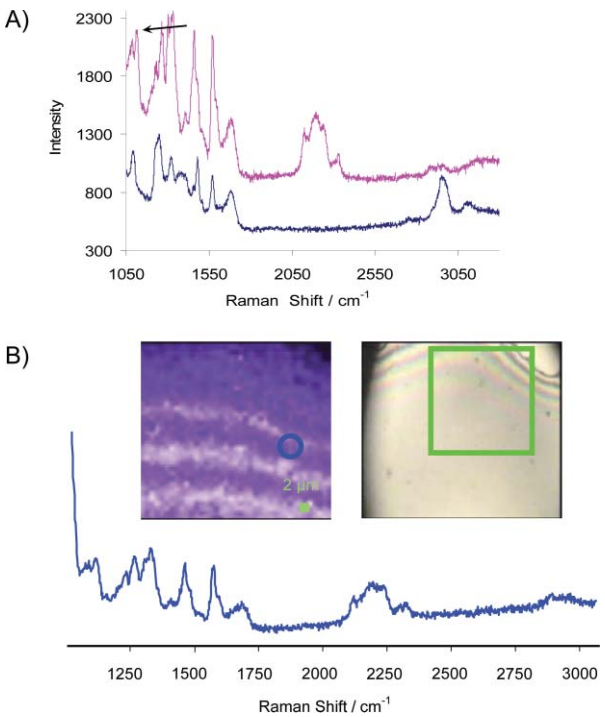

Fig. 4 Raman microscopy analysis of D-HCV RNA. A) Raman spectra of D-HCV RNA (top) and HCV RNA (bottom) illustrating the shift of the aliphatic resonances to the C–D region of the spectrum. The O–P–O nucleotide backbone stretch (1090 cm^{-1}; black arrow) gave confirmation that it was RNA under examination. Spectra were acquired with 5 s integrations from 10 μg μL^{-1} spots that were dried onto a silicon substrate. B) The Raman map (left) shown is a summation of all Raman modes from 2050–2300 cm^{-1}. The striations observed are uncontrolled artefacts acquired during the deposition of D-HCV-RNA onto the silicon substrate. The optical image (right) shows the 40 × 40 μm area that was imaged to create the Raman map. The Raman spectrum shown is from an area of bright intensity in the Raman image, which is indicative of an abundance of C–D modes. This image clearly showed that image contrast specific to the C–D mode of D-HCV RNA could be generated.

Preparation and characterization of aminoallyl uridine HCV RNA and benzonitrile-labeled HCV RNA

Initial investigations into the CN mode focused on acetonitrile as a model compound. Following normalization to 10 mM (which is a conservative estimate of eventual *in vivo* localized probe concentration), the Raman scattering cross-section of acetonitrile was determined to be below current CARS detection limits (data not shown). Therefore, if the CN mode was to be used as a CARS contrast agent, the scattering cross-section needed to be increased. This was achieved by increasing the polarizability of the CN mode by conjugation with an aromatic system. The validity of this approach for generating vibrational image contrast was recently demonstrated using *N*-((4-cyanobenzyl)hydroxyl)succinimide (4-CN-NHS).[27,28]

Building from these studies, ((4-cyanobenzamido)ethyl)-maleimide (4-CN-M) was prepared with the goal of modifying HCV RNA containing a terminal thiol (Fig. 5A). The 5′-CN-modified HCV RNA (5′-CN HCV RNA) was analyzed by electrophoretic comparison with HCV RNA and 5′-fluorescein-modified HCV RNA (5′-F HCV RNA; Fig. 5B). The results implied that the labeling reaction was successful. However, the width of the 5′-labeled RNA bands indicated that theses samples had different chemical properties than unmodified HCV RNA, which may lead to a change in their electrophoretic migration (apparent mass-shift did not correlate with the mass of 5′-F or 5′-CN HCV RNA). This strategy incorporates only one labeled nucleotide into a whole HCV RNA replicon (~10 000 nt), which is below the current Raman/CARS microscopy detection limits. Therefore, we attempted to modify multiple ribonucleobases with Raman labels.

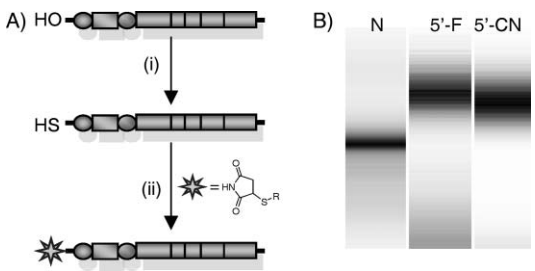

Fig. 5 Synthesis and analysis of 5′-labeled HCV RNA products. A) (i) the 5′-OH is exchanged for a thiophosphate group through the action of T4 polynucleotide kinase (only the thiol has been shown for simplicity); and (ii) the 5′-thiol then reacts *via* 1,4-addition with a maleimide probe to yield 5′-labeled RNA. B) Relative to HCV RNA (N) the electrophoretic migration of 5′-F HCV RNA (5′-F) and 5′-CN HCV RNA (5′-CN) displayed a large mass-shift, indicating a much higher molecular weight, which did not correlate with the mass of fluorescein-M or 4-CN-M.

Labeling nucleotide bases with *N*-hydroxysuccimide-activated benzonitrile compounds necessitated the incorporation of a reactive handle into HCV RNA. A variety of nucleotide analogues have been developed to incorporate additional functionality to DNA and RNA.[37–40] Notable amongst these derivatives is

5-(aminoallyl)uridine (aaU; Fig. 6A), which has been used extensively as a reactive handle to which various tags are conjugated for downstream applications.[41–43]

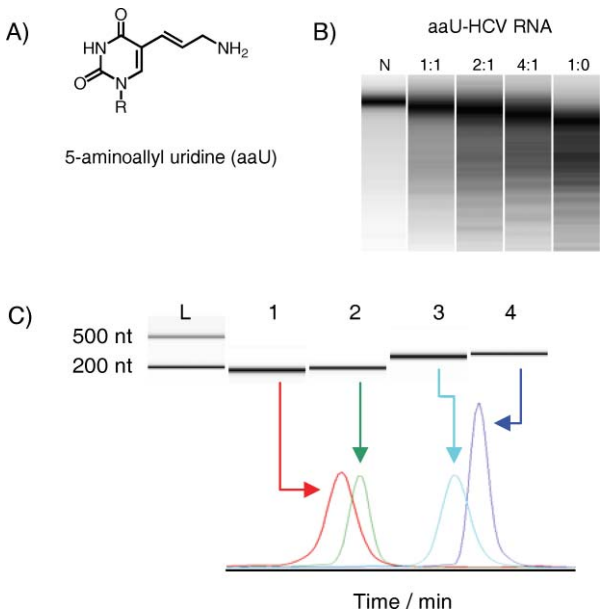

Fig. 6 Validation of aaU-HCV RNA synthesis. A) Structure of aaU. B) Electrophoresis of HCV RNA (N) and aaU-HCV RNA, which was synthesized with increasing ratios of aaUTP:UTP (indicated above the remaining lanes). C) A similar trend in migration was observed for smaller transcripts. Lanes 1 and 3 are aaU-modified 163-mer/270-mer transcripts, respectively. Lanes 2 and 4 are unmodified control transcripts. R = ribose.

The synthesis of aaU-modified HCV RNA (aaU-HCV RNA) was successfully demonstrated, with acceptable yields of 50–70% when compared to normal IVT of HCV RNA (Fig. 6B). Further analysis of the electropherograms revealed that aaU-HCV RNA displayed an abnormal migration velocity relative to unmodified HCV RNA. This observation suggested that either an early termination product was the primary transcript or that the electrophoretic migration of aaU-HCV RNA was altered relative to HCV RNA. A similar trend in migration was observed for aaU-modified 163 nt and 270 nt transcripts (data not shown). This demonstrated that the migration shift was a general consequence of using aaU, and supported the conclusion that the aberrant electrophoretic migration of aaU-HCV RNA was likely due to altered physicochemical properties rather than a predefined early termination site.

In addition to the slower migration velocity, there was a heterogeneous mixture of transcripts present in IVT reactions that used aaUTP (data not shown). This is a common problem when working with modified nucleobases that stems from premature termination of transcription. Importantly, the polymerase used in the current study (T7) has been used to incorporate aaU and other 5-modified uridine derivatives into short *in vitro*-generated transcripts. In these reactions, a significant quantity of early termination products were produced using small (10–50 nt) transcripts and modified nucleotides, including aaU.[33–36] Thus, it was expected that such products would also be produced during the synthesis of larger transcripts (*i.e.*, HCV RNA). By augmenting the ratio of UTP:aaUTP in the IVT reaction the presence of early termination products was minimized (Fig. 6B). Moreover, when a 4 : 1 UTP:aaUTP ratio was used, the electrophoretic migration and sample heterogeneity of the aaU-HCV RNA products were closer to unmodified HCV RNA (Fig. S1A†).

Since a mixture of UTP and aaUTP was used to generate aaU-HCV RNA, the number of aaU residues present in the aaU-HCV RNA transcript was dependant upon the probability of T7 incorporating wild-type *versus* modified substrates. To quantitatively determine the amount of aaU incorportated into aaU-HCV RNA, several techniques were considered. Matrix-assisted laser desorption ionization (MALDI) MS is often used to identify modified ribonucleobases.[44,45] However, there is a size restriction for MALDI-MS analysis of RNA of around 1200 nt, and it is difficult to obtain quantitative data.[46–48] Since HCV RNA is a 10 000 nt transcript and quantitative data is required, MALDI-MS was unsuitable. Two other techniques used to characterize modified ribonucleobases that are capable of providing diagnostic and quantitative data are HPLC and LC-MS.[49–51] However, before transcripts as large as aaU-HCV RNA and benzonitrile-modified aaU-HCV RNA (CN-HCV RNA) could be analyzed they needed to be degraded to their constituent monomers.

An important consideration when designing a protocol for the digestion and dephosphorylation of modified RNAs is the specificity of the nuclease and phosphatase for unnatural substrates. While several studies have used snake venom phosphodiesterase to mediate RNA digestion for HPLC analysis, it was postulated that this enzyme cannot fully degrade RNA containing uridine analogues, including aaU.[36,49–51] As a result, S1 nuclease was chosen to develop this methodology, as it has been shown to efficiently digest alkylated, depurinated and UV-irradiated substrates.[52] S1 is also known to catalyze the digestion of double-stranded and single-stranded RNA segments, which was important due to the highly complex secondary and tertiary structural elements present in HCV RNA.[52]

Once the validity of the digestion/dephosphorylation and HPLC/LC-MS analyses were demonstrated (Fig. S2, S8 and S9), it was possible to investigate the extent of aaU incorporation into aaU-HCV RNA with the surety that the results obtained were representative of the entire modified transcript. Previous studies specifically investigated the efficacy with which T7 incorporated various 5-modified uridine analogues, two of which bear similarities to aaU.[35] In this study, it was found that uridine derivatives bearing a positively charged group (primary amine or histidine) at the 5-position produced full-length transcripts from a sequence designed to be difficult for T7 to transcribe as well or better than reactions using wild-type substrates. This finding fits very well with the experimentally determined aaU:U ratio in aaU-HCV RNA transcripts of 1 : 1.1 to 1 : 1.3, which implied that aaUTP was incorporated more efficiently than UTP. There are 2166 uridines in HCV replicon RNA, which meant that there were 1100–1200 aaU residues incorporated into aaU-HCV RNA. This also meant that there are 1100–1200 reactive primary amines amenable to modification with benzonitrile groups. Additionally, HPLC analysis demonstrated that the extent of aaU incorporation could be regulated by adjusting the amount of aaUTP in the IVT reaction (Fig. S1B).

Repeated attempts at modifying aaU and aaU-HCV RNA with 4-CN-NHS were unsuccessful. Believing this to be a stereoelectronic effect, the labeling reaction was attempted using

N-(benzoyloxy)succinimide (Bz-NHS). HPLC analysis of the aaU monomer, as well as short transcripts and full-length aaU-HCV RNA, confirmed that the reaction proceeded to completion when Bz-NHS was used in place of 4-CN-NHS (Fig. S3 and S4). Bz-NHS labeling was next applied to an aaU-modified 163-mer. Examination of the electrophoretic migrations again indicated a successful reaction, since the increased apparent mass of the labeled RNA was consistent with the chemical conjugation of the benzyl group (Fig. S4).

Next, we successfully labeled aaU-HCV RNA using *N*-((3-cyanobenzyl)hydroxyl)succinimide (3-CN-NHS), which has a relative reactivity between 4-CN-NHS and Bz-NHS. HPLC analysis of the monomer reaction, as well as modification of short and full-length aaU-HCV RNA transcripts, revealed a clear disappearance of the aaU peak and a corresponding appearance of a new eluent that was identified as the CN-modified aaU monomer (Fig. S4 and S5). Also noteworthy from these experiments was the finding that >90% labeling efficiency was achieved for all RNA modification reactions. This translates into approximately 10% (*ca.* 1000 nt) of the HCV replicon RNA that were modified with benzonitrile contrast agents.

To further confirm the benzonitrile modification of aaU-HCV RNA, Raman imaging of CN-HCV RNA was conducted. Analysis revealed a spectrally well-resolved signal corresponding to the CN mode at 2238 cm^{-1} (Fig. 7A), whereas the 1050–2000 cm^{-1} and 2800–3000 cm^{-1} regions retained all the spectroscopic information of HCV RNA. Additionally, image contrast specific to CN-HCV RNA could be generated by integrating the Raman image from 2200–2260 cm^{-1} (Fig. 7B). Similar to D-HCV RNA, *in vivo* imaging was hindered due to the sensitivity limits associated with cellular imaging using Raman microscopy. However, when coupled with the HPLC/LC-MS data presented thus far, the Raman data indicated that the modification of aaU-HCV RNA with 3-CN-NHS was successful.

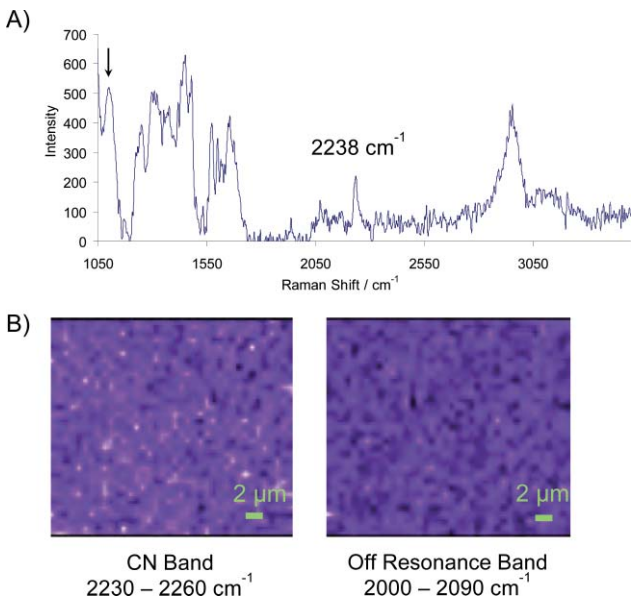

Fig. 7 Raman microscopy analysis of CN-HCV RNA. A) A clear peak at 2238 cm^{-1} was final evidence that the 3-CN-NHS modification of aaU-HCV RNA was successful. Also evident was the O–P–O nucleotide backbone resonance at 1090 cm^{-1} (arrow), which gave confirmation that it was RNA under examination. B) Raman image contrast was generated by integrating the CN band from 2230–2260 cm^{-1}. An intensity difference was observed when compared to an off-resonance image.

Biophysical characterization of aaU-HCV RNA and CN-HCV RNA

Dynamic light scattering (DLS) is a spectroscopic technique used primarily to size particle suspensions. In particular, due to the intense scattering of light from the metallic surface, DLS has been used extensively to characterize colloidal nanoparticle solutions to measure the degree of polydispersion.[53] DLS has also been used to characterize the hydrodynamic radius of biomolecules, including proteins, lipids and oligonucleotides.[54–59] As a first-line means of investigating the structural effects of modifying HCV RNA, the hydrodynamic radii of modified HCV RNAs were measured. The results showed negligible differences between the modified RNAs (D-HCV RNA, aaU-HCV RNA and CN-HCV-RNA) and HCV RNA (Fig. S6).

Atomic force microscopy (AFM) has been used extensively in the study of DNA. Recently, it was extended to the investigation of RNA secondary structure and viral RNAs.[60–68] We employed AFM to investigate the bulk structural effects of modification to aaU-HCV RNA and CN-HCV RNA relative to HCV RNA. These samples are the most amenable to study with AFM because the nature of their modifications imply that they would experience the largest structural perturbations and were, therefore, likely to be within the resolution limits of AFM.

To facilitate the adhesion of polyanionic RNA to the anionic mica surface, a sufficient concentration of Mg^{2+} (mM) must be present in the AFM analysis buffer to overcome the coulobmic repulsion between the like charges of RNA and mica.[69,70] The apparent radii of the modified RNAs following surface deposition appeared similar, with the dispersion consistently ranging from 80–120 nm. It is well established that during deposition long polymers often undergo 3D-to-2D transition.[71] This is caused by partial dissolution of the condensed state due to interactions with surface Mg^{2+} that become energetically favorable as the deposition buffer is removed. The discrepancy between the AFM and DLS radii was likely the result of these transitions.

The morphology of the RNA following deposition provided valuable information regarding the structural changes introduced into aaU-HCV RNA and CN-HCV RNA. While the observed condensed state was not representative of native tertiary structure, it contained non-specific structural elements that could be used as a model for the effects of labeling on native HCV RNA structure.[69] Comparison of the AFM images acquired for aaU-HCV RNA, CN-HCV RNA and HCV RNA revealed distinct differences in morphology that implied the modified RNAs adopted a more open conformation on the mica surface (Fig. 8). Also, single-stranded RNA fragments were observed with higher frequency for the modified RNAs.

These results were best explained by considering the energetics of the condensed state tertiary (and possible secondary) structural elements in the modified *versus* unmodified RNAs. The morphology of HCV RNA suggested a tightly packed condensed state in which non-specific tertiary interactions were largely maintained during the deposition process. Energetically this meant that the Mg^{2+}-induced non-specific tertiary interactions

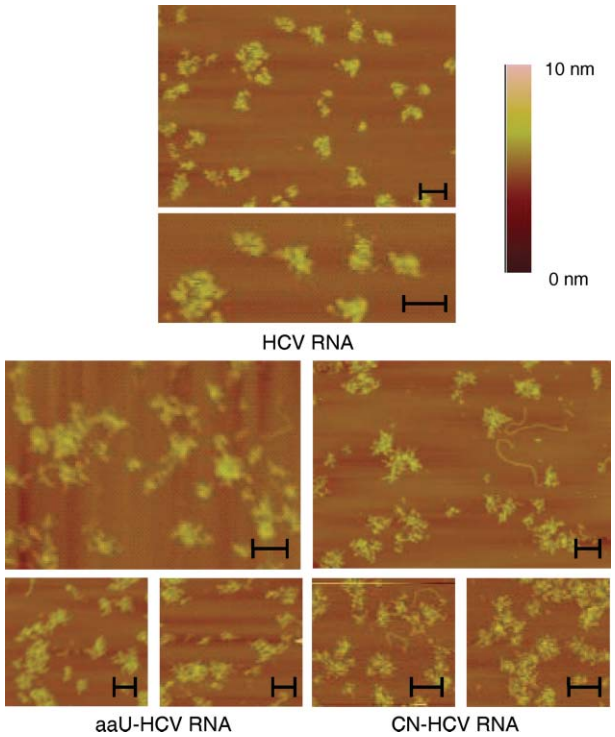

Fig. 8 AFM analysis of modified HCV RNAs. Unmodified HCV RNA appeared as tight clusters, indicating that non-specific tertiary interactions in the collapsed state remained intact. The presence of single-stranded segments and generally more relaxed appearance of aaU-HCV RNA and CN-HCV RNA implied that the collapsed state tertiary interactions were dissociating in favor of coordinating with surface Mg^{2+}. This was concluded to be a direct result of aaU and aaU-CN destabilizing these interactions such that coordinating with surface Mg^{2+} was energetically favored. All scale bars are 100 nm.

were more favorable than RNA interactions with the Mg^{2+}-coated mica surface. Application of identical reasoning to the images of aaU-HCV RNA and CN-HCV RNA led to the conclusion that the non-specific tertiary interactions in the condensed states were weakened as result of the modifications introduced to enable live-cell RNA tracking using Raman/CARS microscopy. Thus, the more relaxed conformation of the modified RNAs showed that Mg^{2+}-induced intramolecular interactions were energetically higher than interactions with the Mg^{2+}-coated mica surface.

Functional validation of modified HCV RNAs

The structural complexity of the HCV genome underscores the importance of characterizing the functional and structural consequences of biomolecular modification. Such investigations are especially relevant to the present study because research shows that subtle changes to the primary sequence of HCV RNA can result in drastic functional consequences.[72–75] It follows from this that incorporating a heavily modified nucleotide analogue throughout the length of the genome was likely to have significant deleterious effects. Owing to this, functional validation of the modified HCV RNAs using a luciferase reporter gene was performed.

In the presence of Mg^{2+}, ATP and the beetle luciferin substrate, the luciferase protein catalyzes the production of light, and the amount of light produced can be correlated to the amount of luciferase that was translated *in vivo*.[11,76] We utilized an HCV replicon system containing the luciferase gene under the control of an HCV IRES.[13] With this system, changes in luciferase expression can be directly correlated to translational perturbations and indirectly correlated to replicative changes that resulted from the modifications introduced to enable tracking by Raman and CARS microscopy.

The expression of the luciferase reporter gene was investigated following RNA modification at the transcriptional and post-transcriptional level (Fig. 9). The results showed that the luciferase activity was severely affected for aaU-HCV RNA (5%), CN-HCV RNA (15%), 5′-CN HCV RNA (20%) and 5′-F HCV RNA (50%) when compared to unmodified HCV RNA. In contrast, D-HCV RNA maintained approximately 60% of wild-type luciferase activity when contrasted against unmodified HCV RNA. The fact that these trends continued through the 48 hour time-point was indicative of a replicative and/or translational deficiency introduced by the modification of HCV RNAs.

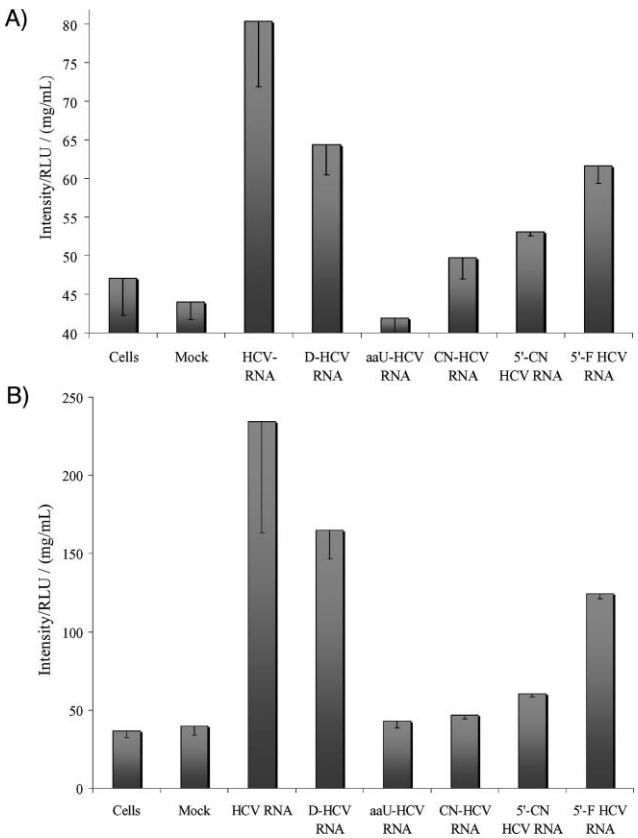

Fig. 9 Luciferase activity of modified HCV RNAs. 24 h (A) and 48 h (B) endpoints were examined. Data showed that aaU-HCV RNA, CN-HCV RNA and 5′-CN HCV RNA suffered severe functional deficits as a result of modification. Mock treatment was with transfection reagent only. All measurements were made in triplicate and are reported as mean values ± one standard deviation.

These results suggest that although the incorporation of benzonitrile groups into HCV RNA is possible, the functional consequences of these modifications preclude their use in live-cell imaging. Conversely, C–D bonds appear to function as reasonable vibrational labels while retaining the function of the HCV replicon. Furthermore, when HCV RNA transcripts containing one of

the deuterated nucleosides per IVT reaction were analyzed, the luciferase activity of G/C and A/U substitutions clearly deviated from each other and showed that the activity of D-HCV RNA could be increased to near wild-type levels (Fig. S7).

It should be noted that the decreased luciferase activity in these modified RNAs can be attributed to a variety of sources—decreased transfection efficiency, RNA stability, altered RNA–RNA or RNA–protein interactions, *etc.* However, while the precise cause is unclear, the AFM data presented herein suggested that the decreased luciferase activity was causally linked to structural perturbations introduced upon modification of the HCV RNA.

Conclusions

In summary, the incorporation of deuterium and CN Raman modes into very large HCV RNA molecules was carried out to establish a means of tracking processes related to RNA processing, motility and localization using Raman/CARS microscopy. Characterizations of these materials by HPLC and LC-MS demonstrated the validity of the methodologies used to incorporate these endogenous Raman modes into HCV RNA. Additionally, Raman microscopy and spectroscopy provided evidence that contrast specific to C–D and CN modes could be generated, suggesting that these materials could be used to track modified RNAs *in vivo*. Although the nitrile functionality has a stronger Raman cross-section than the C–D bond, D-HCV RNA has the least perturbation to HCV replicon function relative to unmodified HCV RNA. The results presented here provide a solid framework for understanding the response of HCV replicon RNA to modifications, and demonstrated that HCV RNA functionalized with C–D and CN modes can be specifically visualized by tuning to these modes using confocal Raman microscopy. Furthermore, given the advantages of CARS microscopy, the Raman imaging experiments indicate that CARS microscopy would be well suited to investigating C–D- and CN-modified biomolecules.

Experimental

Materials and methods

All chemicals were purchased from Aldrich (Oakville, ON, Canada) and used as received. Eighteen megaohm H_2O was obtained from a NANOpure® DIamond™ Life Science Series 1370 water filtration system (Barnstead International, Dubuque, IO, USA) and was used for all applications not requiring RNase-free conditions. The $pFK_{I389}luc/NS3\text{-}3'/5.1$ plasmid, which codes for the HCV subgenomic replicon, was obtained from Ralph Bartenschlager (Institute of Hygiene, University of Heidelberg, Germany). Huh-7 cells were generously provided by Lubica Supekova (Scripps Research Institute, USA). RNA quantification was performed on a ND-1000 spectrophotometer (NanoDrop Technologies, Rockland, DE, USA) and RNA integrity was verified by electrophoresis using the Agilent 2100 bioanalyzer with the RNA LabChip® Nano and Pico kits according to the manufacturer's protocol (Agilent Technologies, Palo Alto, CA, USA). RNA migration behavior and the heterogeneity of transcript populations were determined using the gel and electropherogram functions of the 2100 Expert software, respectively (Agilent Technologies). The synthesis of the benzonitrile labels is described in the Electronic supporting information† and the literature.[28]

Cell culture

Huh-7 cells were cultured at 37 °C and 5% CO_2 in complete cell culture medium that consisted of Dulbecco's modified Eagle medium (DMEM; Invitrogen, Burlington, ON, Canada) supplemented with 10% (v/v) fetal bovine serum (FBS; Cansera International, Rexdale, ON, Canada), 100 nM minimal essential medium nonessential amino acids (Invitrogen), 50 U mL^{-1} penicillin and 50 μg mL^{-1} streptomycin (Invitrogen).

In vitro transcription

HCV RNA was generated using the MEGAscript(tm) IVT kit (Ambion Incorporated, Austin, TX, USA). In brief, $pFK_{I389}luc/NS3\text{-}3'/5.1$ template DNA was linearized with the Sca I restriction enzyme (New England BioLabs, Pickering, ON, Canada). Following an ethanol precipitation, the linearized vector was resuspended in RNase-free H_2O (Ambion) to a final concentration of 0.5 μg μL^{-1}. The transcription reaction was set up according to the manufacturer's protocol and incubated at 37 °C for 2 hours. Additionally, the pTriEx-4 Neo vector (EMD Biosciences Incorporated, San Diego, CA, USA) was digested with Nco I and Sma I restriction enzymes to yield template DNA that produced 163-mer and 270-mer RNA transcripts, respectively, following IVT as described above.

To generate transcripts incorporating aaU (Aldrich), a 1 : 1 (v/v) mixture of 75 mM UTP and 75 mM aaUTP (Aldrich) was prepared and used in place of UTP in the IVT reaction—all other steps were performed as above. To generate deuterated HCV replicon RNA (D-RNA), perdeuterated rNTPs (50 mM; Silantes GmbH, München, Germany) were substituted for normal rNTPs in the transcription reaction—all other steps were performed as above. For transcripts containing only one of the deuterated rNTPs, the appropriate nucleotide was substituted with the deuterated analogue and the IVT reaction was performed as above. All transcripts were cleaned using a MEGAclear™ RNA purification kit (Ambion) according to the manufacturer's protocol.

RNA labeling

HCV RNA transcripts were conjugated to either fluorescein (32 mM; Vector Laboratories, Burlingame, CA, USA) or 4-CN-M (32 mM), which were dissolved in RNase-free DMSO (Aldrich), with the 5′ EndTag™ Nucleic Acid Labeling System (Vector Laboratories) according to the manufacturer's protocol. Following purification by phenol extraction, the labeled RNA was analyzed for quantity and integrity as outlined above.

To label the reactive amine presented by aaU, 3-CN-NHS, 4-CN-NHS and Bz-NHS were utilized. In a typical reaction, 10 μg of RNA containing aaU (or approximately 100 nmol of aaU mononucleoside) was dissolved in labeling reaction buffer (30 mM $NaHCO_3$, pH 9). Following this, an equal volume of 25 mM NHS-activated label in RNase-free DMSO was added. After 1 hour at 37 °C, the reaction was diluted 1 : 10 with RNase-free H_2O and purified by passage through a YM10 MWCO filter (Millipore, Billerica, MA, USA). Following two RNase-free H_2O washes

the collected retentate was analyzed for quantity and integrity as outlined above.

RNA digestion and dephosphorylation

RNA (modified and unmodified) was digested with S1 nuclease (Invitrogen) to afford the constituent mononucleotides. In a typical reaction, 5 μg of RNA was incubated with 50 U of S1 in 30 mM sodium acetate, 1 mM zinc acetate and 5% (v/v) glycerol, pH 4.6 at 37 °C. Digestions were stopped at 1, 2, 4, 8 and 24 hours by passage through a YM10 MWCO filter to examine the time-dependence of the digestion reaction. All other digestion reactions were incubated for 24 hours and subsequently used without purification. Additionally, the concentration-dependence of RNA digestion was investigated by conducting the digestion reaction with 2, 10 and 25 U of S1.

The mononucleotide solution was dephosphorylated by adjusting the buffer conditions to 100 mM NaCl, 50 mM Tris-HCl, 10 mM $MgCl_2$ and 1 mM dithiothreitol, and adding 50 U of calf intestinal phosphatese (New England Biolabs). Following incubation at 37 °C for 24 hours, the constituent mononucleosides were analyzed by HPLC and LC-MS.

HPLC and LC-MS analysis

HPLC was performed on an Agilent 1100 Series LC system equipped with a Waters SunFire™ C18 reverse-phase column (3.5 μm, 2.1 × 100 mm; Waters Corporation, Milford, MA, USA). The elution gradient used was adapted from previous studies investigating RNA by HPLC.[49–51] Resolution was achieved by using a MeOH–0.1 M NH_4OAc, pH 6.5 mixed mobile phase running at 0.2 mL min^{-1} as follows (percent MeOH, elapsed time in min): 1, 0; 10, 15; 50, 16; 50, 20; 95, 30; 95, 35. The elution gradient was linear over all intervals. Typically, 15% (by volume) of a 5 μg HCV-RNA digestion/dephosphorylation reaction was analyzed per HPLC run.

LC-MS was carried out on a Waters 2795 Separations equipped with the above outlined Waters SunFire™ C18 reverse-phase column. In-line monitoring of column eluate was achieved by detection with a Waters 996 photodiode array detector set to 254 nm and a Waters Micromass ZQ 2000 MS. The MS was set to positive ion electrospray detection, with the following defined parameters: capillary voltage: 3.50 kV; cone voltage: 10 V; source temperature: 80 °C; desolvation temperature: 200 °C; desolvation gas flow: 347 L h^{-1}; cone gas flow: 49 L h^{-1}; scan time: 0.5 s; mass range: 100 to 1000. Elution conditions were the same as for HPLC.

Standard curves of absorbance as a function of concentration were constructed for C, U, aaU, G and A (Aldrich) from 0.01–1 mM. The extent of aaU incorporation and 3-CN-NHS modification of RNA containing aaU was quantified using the U and aaU standard curves. Concentrations of the constituent nucleotides following RNA digestion and dephosphorylation were also determined using the standard curves. This data was then used to establish the percentage of RNA that was digested.

Transfection of RNA

For transient expression of pFK_{I389}luc/NS3-3′/5.1-derived HCV RNA, Huh-7 cells were seeded at 5.0×10^4 cells per well in a 24-well plate in 500 μL of complete Huh-7 medium. Cells were transfected once they reached 90% confluency (usually around 24 hours post-seeding). Prior to transfection cells were washed once with phosphate-buffered saline (PBS; 137 mM NaCl, 2.7 mM KCl, 10.1 mM Na_2HPO_4, 1.8 mM KH_2PO_4, pH 7.4) and placed in FBS- and antibiotic-free DMEM at 37 °C while preparing transfection complexes.

Transfection complexes were prepared by mixing 500 ng of RNA with 3.0 μL of DMRIE-C transfection reagent (Invitrogen) in 500 μL per well of FBS- and antibiotic-free DMEM in a 24-well plate as per the manufacturer's protocol. After 4 hours of exposure to the transfection complexes, one equivalent (by volume) of antibiotic-free DMEM containing 20% (v/v) FBS and 100 nM minimal non-essential amino acids were added. Transfected cells were then incubated at 37 °C and 5% CO_2 until desired endpoint(s). All transfection conditions were performed in triplicate.

Cell lysis, luciferase assay and protein quantification

All luciferase assays were performed on lysates from 24-well cell cultures. At the desired time, post-transfection cells were washed once with PBS and subsequently lysed by the addition of 100 μL of 1× cell culture lysis buffer (Promega Corporation, Madison, WI, USA) per well. After 20 min at room temperature the cells were kept at −20 °C for 24 hours to aid lysis.

Luciferase assay substrate (25 mM glycylglycine, 15 mM KH_2PO_4, 4 mM EGTA, 2 mM ATP, 1 mM dithiothreitol, 15 mM $MgSO_4$, 0.1 mM acetyl CoA, and 75 μM beetle luciferin, pH adjusted to 8.0) was prepared fresh prior to use[76]. Forty microlitres of each cellular lysate was transferred to a Microlite white 96-well plate (VWR International, Mississauga, ON, Canada) and the luciferase activity was measured on an Lmax luminometer (Molecular Devices, Sunnyvale, CA, USA) equipped with SOFTmax Pro for Lmax 1.1 L software (Molecular Devices). The following parameters were used for data acquisition: 50 μL of luciferase substrate was injected into each well, followed by a 2 s delay and finally a 10 s integration to quantify the relative light units (RLU) produced.

Total protein content of cellular lysates was quantified using the Bio-Rad DC Protein Assay (Bio-Rad Laboratories, Mississauga, ON, Canada) as per the manufacturer's instructions, with BSA (Aldrich) as the protein standard. The absorbance was read using a BioPhotometer (Eppendorf, Mississauga, ON, Canada) at 595 nm after 15 min of incubation at room temperature. All luciferase and protein data was collected in triplicate. The luciferase signal was normalized against protein content and is presented as mean values ± one standard deviation.

Raman spectroscopy and microscopy

All samples for Raman analysis were analyzed on a phosphorus-doped N-type silicon substrate (single-side polished, 250 ± 25 μm thickness; Virginia Semiconductor Incorporated, Fredericksburg, VA, USA). Raman spectroscopy and microscopy were carried out using a confocal Raman microscope (Horiba Jobin Yvon, Edison, NJ, USA) aligned in a back scattering configuration, which was coupled to an Olympus BX51 microscope (Olympus America Incorporated, Center Valley, PA, USA). Scattered light was collected through a high numerical aperture ($N_a = 0.95$) 100× objective (Olympus) and was detected on a 1024 × 256 element

thermo-electrical cooled CCD detector (Andor Technology, South Windsor, CT, USA). Sample excitation was achieved by a HeNe laser ($\lambda = 632.8$ nm) sharply focused to a diffraction-limited spot, with a focal power density of approximately 10^5 W cm^{-2} (10 mW focused to 1 μm^2). Typically, spectra were acquired with three accumulations of 20 s, with multiple accumulations serving to improve the overall spectral signal-to-noise ratio, as well as allowing the spectral processing software to efficiently remove cosmic spikes. All spectral processing was performed within the manufacturer's instrumental control software, LabSpec 5.04 (Horiba Jobin Yvon). Spectral smoothing was achieved using the Savitsky–Golay smoothing routine.

Atomic force microscopy

For imaging, RNA was diluted in AFM imaging buffer (40 mM HEPES, 10 mM $MgCl_2$, pH 7.0) to 2–5 ng μL^{-1}. Five microlitres of the diluted RNA solution was dropped onto freshly cleaved mica (grade V2; Ted Pella Incorporated, Redding, CA, USA) and allowed to adsorb for 5 min at room temperature. Non-absorbed RNA was removed by washing three times with RNase-free H_2O (500 μL per wash), after which the sample was dried under a stream of nitrogen. Imaging was performed under ambient conditions in tapping mode on a NanoScope IIIa atomic force microscope (Digital Instruments, Woodbury, NY, USA) equipped with an E-piezoscanner (Digital Instruments). Pointprobe® plus non-contact, high-resonance frequency tips (Nanosensors, Neuchatel, Switzerland), with a force constant of 21–78 N m^{-1} and a resonance frequency of 260–410 kHz, were used for all measurements. Fields of 0.5–3.0 μm were scanned at 1–1.5 Hz. Images were flattened and approximate cluster diameters were determined using NanoScope v5.12r4 software (Digital Instruments). The same software was used to manually determine cluster diameters. Following imaging, all diluted RNA was analyzed to verify integrity.

Dynamic light scattering

DLS measurements were recorded on a Zetasizer 3000 HSA (Malvern Instruments Limited, Worcestershire, UK). Scattered light was produced by a 633 nm incident beam and was detected at an angle of 90° and a temperature of 25 °C. All measurements were taken in a Quartz SUPRASIL cuvette (Hellma GmbH & Co KG, Müllheim, Germany) with a 3 mm path length and 45 μL sample volume. Samples were prepared in AFM imaging buffer and allowed to incubate for 10 min at room temperature prior to measurement. The integrity of all RNA was verified following analysis. Data is reported as the mean hydrodynamic radius (nm) ± the polydispersion factor calculated by the Zetasizer software.

Acknowledgements

We thank Y. Rouleau and S. Belanger for their assistance in preparing IVTs and M. Tomietto for assistance with AFM experiments. We thank the Canadian Institutes for Health Research (CIHR) for financial support of this work.

References

1 Q. Choo, G. Kuo, A. Weiner, L. Overby, D. Bradley and M. Houghton, *Science*, 1989, **244**, 359–362.
2 World Health Organization, http://www.who.int/mediacentre/factsheets/fs164/en/index.html, revised November 2000.
3 P. Simmonds, *J. Gen. Virol.*, 2004, **85**, 3173–3188.
4 R. Bartenschlager and V. Lohmann, *Antiviral Res.*, 2001, **52**, 1–17.
5 D. F. Mercer, D. E. Schiller, J. F. Elliott, D. N. Douglas, C. Hao, A. Rinfret, W. R. Addison, K. P. Fischer, T. A. Churchill, J. R. T. Lakey, D. L. J. Tyrrell and N. M. Kneteman, *Nat. Med.*, 2001, **7**, 927–933.
6 Z. Hong, M. Beaudet-Miller, R. E. Lanford, B. Guerra, J. Wright-Minogue, A. Skelton, B. M. Baroudy, G. R. Reyes and J. Y. N. Lau, *Virology*, 1999, **256**, 36–44.
7 B. Bartosch, J. Dubuisson and F.-L. Cosset, *J. Exp. Med.*, 2003, **197**, 633–642.
8 M. Hsu, J. Zhang, M. Flint, C. Logvinoff, C. Cheng-Mayer, C. M. Rice and J. A. McKeating, *Proc. Natl. Acad. Sci. U. S. A.*, 2003, **100**, 7271–7276.
9 B. D. Lindenbach, M. J. Evans, A. J. Syder, B. Wolk, T. L. Tellinghuisen, C. C. Liu, T. Maruyama, R. O. Hynes, D. R. Burton, J. A. McKeating and C. M. Rice, *Science*, 2005, **309**, 623–626.
10 T. Wakita, T. Pietschmann, T. Kato, T. Date, M. Miyamoto, Z. Zhao, K. Murthy, A. Habermann, H.-G. Krausslich, M. Mizokami, R. Bartenschlager and T. J. Liang, *Nat. Med.*, 2005, **11**, 791–796.
11 N. Krieger, V. Lohmann and R. Bartenschlager, *J. Virol.*, 2001, **75**, 4614–4624.
12 S. M. Sagan, Y. Rouleau, C. Leggiadro, L. Supekova, P. G. Schultz, A. I. Su and J. P. Pezacki, *Biochem. Cell Biol.*, 2006, **84**, 67–79.
13 B. Rakic, S. M. Sagan, M. Noestheden, S. Belanger, X. Nan, C. L. Evans, X. S. Xie and J. P. Pezacki, *Chem. Biol.*, 2006, **13**, 23–30.
14 V. Lohmann, F. Körner, J.-O. Koch, U. Herian, L. Theilmann and R. Bartenschlager, *Science*, 1999, **285**, 110–113.
15 S. P. Wheatley and Y. L. Wang, *Methods Cell Biol.*, 1998, **57**, 313–332.
16 J. M. Levsky and R. H. Singer, *J. Cell Sci.*, 2003, **116**, 2833–2838.
17 A. M. Femino, F. S. Fay, K. Fogarty and R. H. Singer, *Science*, 1998, **280**, 585–590.
18 R. W. Dirks, C. Molenaar and H. J. Tanke, *Methods*, 2003, **29**, 51–57.
19 R. Gosert, D. Egger, V. Lohmann, R. Bartenschlager, H. E. Blum, K. Bienz and D. Moradpour, *J. Virol.*, 2003, **77**, 5487–5492.
20 Q. Li, Y. Kim, J. Namm, A. Kulkarni, G. R. Rosania, Y.-H. Ahn and Y.-T. Chang, *Chem. Biol.*, 2006, **13**, 615–623.
21 M. M. Mhlanga, D. Y. Vargas, C. W. Fung, F. R. Kramer and S. Tyagi, *Nucleic Acids Res.*, 2005, **33**, 1902–1912.
22 J. S. Andersen, Y. W. Lam, A. K. L. Leung, S.-E. Ong, C. E. Lyon, A. I. Lamond and M. Mann, *Nature*, 2005, **433**, 77–83.
23 E. Bertrand, P. Chartrand, M. Schaefer, S. M. Shenoy, R. H. Singer and R. M. Long, *Mol. Cell*, 1998, **2**, 437–445.
24 X. Nan, A. Tonary, M. A. Stolow, X. S. Xie and J. P. Pezacki, *ChemBioChem*, 2006, **12**, 1895–1857.
25 H. Aizaki, K. Choi, M. Liu, Y.-j. Li and M. Lai, *J. Biomed. Sci.*, 2006, 1–12.
26 K. C. Schultz, L. Supekova, Y. Ryu, J. Xie, R. Perera and P. G. Schultz, *J. Am. Chem. Soc.*, 2006, **128**, 13984–13985.
27 Q. Hu, L. L. Tay, M. Noestheden and J. P. Pezacki, *J. Am. Chem. Soc.*, 2007, **129**, 14–15.
28 M. Noestheden, Q. Hu, L. L. Tay, A. Tonary, A. Stolow, R. Mackenzie, J. Tanha and J. P. Pezacki, *Bioorg. Chem.*, 2007, **35**, 284–293.
29 I. T. Suydam and S. G. Boxer, *Biochemistry*, 2003, **42**, 12050–12055.
30 N. Johnsson, N. George and K. Johnsson, *ChemBioChem*, 2005, **6**, 47–52.
31 P. F. van Swieten, M. A. Leeuwenburgh, B. M. Kessler and H. S. Overkleeft, *Org. Biomol. Chem.*, 2005, **3**, 20–27.
32 J. L. Meier, A. C. Mercer, H. Rivera and M. D. Burkart, *J. Am. Chem. Soc.*, 2006, **128**, 12174–12184.
33 H. B. Gamper, A. Gewirtz, J. Edwards and Y.-M. Hou, *Biochemistry*, 2004, **43**, 10224–10236.
34 R. Kawai, M. Kimoto, S. Ikeda, T. Mitsui, M. Endo, S. Yokoyama and I. Hirao, *J. Am. Chem. Soc.*, 2005, **127**, 17286–17295.
35 J. D. Vaught, T. Dewey and B. E. Eaton, *J. Am. Chem. Soc.*, 2004, **126**, 11231–11237.
36 T. Schoetzau, J. Langner, E. Moyroud, I. Roehl, S. Vonhoff and S. Klussmann, *Bioconjugate Chem.*, 2003, **14**, 919–926.
37 D. E. Bergstrom and J. L. Ruth, *J. Am. Chem. Soc.*, 1976, **98**, 1587–1589.
38 J. L. Ruth and D. E. Bergstrom, *J. Org. Chem.*, 1978, **43**, 2870–2876.
39 D. E. Bergstrom and M. L. Ogawa, *J. Am. Chem. Soc.*, 1978, **100**, 8106–8112.
40 J. Inoue and T. Ueda, *Chem. Pharm. Bull.*, 1978, **26**, 2657–2663.

41 C. Chen, M. Gorin and D. Sigman, *Proc. Natl. Acad. Sci. U. S. A.*, 1993, **90**, 4206–4210.
42 P. A. C. 't Hoen, F. de Kort, G. J. B. van Ommen and J. T. den Dunnen, *Nucleic Acids Res.*, 2003, **31**, e20.
43 C. C. Xiang, O. A. Kozhich, M. Chen, J. M. Inman, Q. N. Phan, Y. Chen and M. J. Brownstein, *Nat. Biotechnol.*, 2002, **20**, 738–742.
44 F. Kirpekar, S. Douthwaite and P. Roepstorff, *RNA*, 2000, **6**, 296–306.
45 K. A. Kellersberger, E. T. Yu, S. I. Merenbloom and D. Fabris, *J. Am. Soc. Mass Spectrom.*, 2005, **16**, 199–207.
46 S. Berkenkamp, F. Kirpekar and F. Hillenkamp, *Science*, 1998, **281**, 260–262.
47 A. Ke and J. A. Doudna, *Methods*, 2004, **34**, 408–414.
48 F. Kirpekar and T. N. Krogh, *Rapid Commun. Mass Spectrom.*, 2001, **15**, 8–14.
49 M. Buck, M. Connick and B. N. Ames, *Anal. Biochem.*, 1983, **129**, 1–13.
50 P. F. Crain, *Methods Enzymol.*, 1990, **193**, 782–790.
51 S. C. Pomerantz and J. A. McCloskey, *Methods Enzymol.*, 1990, **193**, 796–824.
52 N. A. Desai and V. Shankar, *FEMS Microbiol. Rev.*, 2003, **26**, 457–491.
53 A. Panacek, L. Kvitek, R. Prucek, M. Kolar, R. Vecerova, N. Pizurova, V. K. Sharma, T. Nevecna and R. Zboril, *J. Phys. Chem. B*, 2006, **110**, 16248–16253.
54 J. Langowski and U. Giesen, *Biophys. Chem.*, 1989, **34**, 9–18.
55 K. G. Reddie, D. R. Roberts and T. M. Dore, *J. Med. Chem.*, 2006, **49**, 4857–4860.
56 J. Guo, N. Harn, A. Robbins, R. Dougherty and C. R. Middaugh, *Biochemistry*, 2006, **45**, 8686–8696.
57 M. Ruponen, C. S. Braun and C. R. Middaugh, *J. Pharm. Sci.*, 2006, **95**, 2101–2114.
58 D.-M. Zhu and R. K. Evans, *Langmuir*, 2006, **22**, 3735–3743.
59 J. L. A. A. Timchenko and I. N. Serdyuk, *Biopolymers*, 1993, **33**, 1747–1755.
60 K. Umemura, F. Nagami, T. Okada and R. Kuroda, *Nucleic Acids Res.*, 2000, **28**, e39.
61 Z. Liu, H. Zhou, G. Wei, Y. Song and L. Wang, *Microsc. Res. Tech.*, 2005, **66**, 179–185.
62 H. G. Hansma, K. Kasuya and E. Oroudjev, *Curr. Opin. Struct. Biol.*, 2004, **14**, 380–385.
63 H. G. Hansma, E. Oroudjev, S. Baudrey and L. Jaeger, *J. Microsc.*, 2003, **212**, 273–279.
64 O. Medalia, M. Heim, R. Guckenberger, R. Sperling and J. Sperling, *J. Struct. Biol.*, 1999, **127**, 113–119.
65 H. G. Hansma, R. Golan, W. Hsieh, S. L. Daubendiek and E. T. Kool, *J. Struct. Biol.*, 1999, **127**, 240–247.
66 Y. G. Kuznetsov, S. Daijogo, J. Zhou, B. L. Semler and A. McPherson, *J. Mol. Biol.*, 2005, **347**, 41–52.
67 A. Giro, A. Bergia, G. Zuccheri, H. H. J. Bink, C. W. A. Pleij and B. Samorì, *Microsc. Res. Tech.*, 2004, **65**, 235–245.
68 Y. F. Drygin, O. A. Bordunova, M. O. Gallyamov and I. V. Yaminsky, *FEBS Lett.*, 1998, **425**, 217–221.
69 D. E. Draper, D. Grilley and A. M. Soto, *Annu. Rev. Biophys. Biomol. Struct.*, 2005, **34**, 221–243.
70 M. L. Sushko, A. L. Shluger and C. Rivetti, *Langmuir*, 2006, **22**, 7678–7688.
71 C. Rivetti, M. Guthold and C. Bustamante, *J. Mol. Biol.*, 1996, **264**, 919–932.
72 H. Lee, H. Shin, E. Wimmer and A. V. Paul, *J. Virol.*, 2004, **78**, 10865–10877.
73 P. Friebe, J. Boudet, J.-P. Simorre and R. Bartenschlager, *J. Virol.*, 2005, **79**, 380–392.
74 F. Odreman-Macchioli, F. E. Baralle and E. Buratti, *J. Biol. Chem.*, 2001, **276**, 41648–41655.
75 P. Friebe, V. Lohmann, N. Krieger and R. Bartenschlager, *J. Virol.*, 2001, **75**, 12047–12057.
76 B. W. Dyer, F. A. Ferrer, D. K. Klinedinst and R. Rodriguez, *Anal. Biochem.*, 2000, **282**, 158–161.